FEATURE ARTICLE

Surface Femtochemistry: Frustrated Desorption of Alkali Atoms from Noble Metals

H. Petek,* H. Nagano, M. J. Weida, and S. Ogawa

Advanced Research Laboratory, Hitachi, Ltd., Hatoyama, Saitama 350-0395, Japan

Received: December 18, 2000; In Final Form: April 9, 2001

The electronic excitation of chemisorbed Cs atoms through the coherent photoinduced charge transfer from the Cu(111) surface turns on repulsive forces that initiate the dissociative wave packet motion. Due to unusually slow electronic relaxation, with the interferometric time-resolved two-photon photoemission technique it is possible to follow the characteristic change in the surface electronic structure due to the ensuing nuclear dynamics for ∼200 fs after excitation. This direct observation of the incipient bond breaking process on a metal surface provides information on a series of complex electronic and nuclear events that previously could be gleaned only through analysis of the reaction products. The metal band structure, the polarizability of the Cs atom, and the mechanical properties of the surface strongly influence the electronic and nuclear relaxation, and therefore, the reaction efficiency. The importance of time-resolved methods in studying of surface reactions is underscored by significant deviations in the electronic and nuclear dynamics of Cs/Cu(111) from the standard models for surface photochemistry.

I. Introduction

Observation of transition states in surface chemical reactions is one of the Holy Grails in chemistry.[1,2] With state-of-the-art laser technology, it is now possible to follow in real-time nuclear motions of even light atoms in the course of simple gas-phase unimolecular and bimolecular reactions.[1−5] Time-evolution of nuclear wave packets created by impulsive laser excitation of molecules can be probed by ultrafast spectroscopic or diffraction techniques.[1,2] With optical techniques, it is even possible to exert control of photochemical reactions through quantum interference, or multiphoton excitation.[6−8]

Nearly perfect translational and orientational order imposed on adsorbed reactants is a uniquely attractive feature of single-crystal surfaces for studies of transition state dynamics.[1] Moreover, the importance of surface and interface chemistry to many fields of science and technology provides a strong motivation for charting the topography of potential energy surfaces in heterogeneous media. Although gas-phase studies provide a valuable experimental and theoretical context for discussing the transition state dynamics, the substrate inevitably introduces significant complexity that is intrinsic to solid-state systems.[9−13]

The possibility of observation of transition state dynamics on surfaces via traditional surface science techniques is subverted by the limited density of adsorption sites and extremely fast relaxation rates. The main recourse to probing the transition state dynamics has been to record the flux, velocity, alignment, and internal state distributions of the gas-phase products.[9−11,14−17] However, such postmortem studies provide only indirect information on the transition state topography and electronic and nuclear relaxation processes based on a severe framework of approximations.[14]

Ultrafast laser techniques provide a more direct approach to observing short-lived surface species in the course of a chemical raction.[18] Here the interferometric time-resolved two-photon photoemission (ITR-2PP) technique is applied to one of the ostensibly simplest surface chemical reactions, namely, desorption. ITR-2PP provides a detailed picture of the evolution of the electronic and nuclear structure preceding Cs atom desorption from the Cu(111) surface for 200 fs following photoexcitation.[19−27]

II. Surface Photochemistry

Electronic excitation of surface adsorbates initiates a chain of events generically known as desorption induced by electronic transition (DIET).[9−11,14,28−31] Being nearly instantaneous, electronic excitation impulsively turns on forces, which induce nuclear motion leading to a chemical reaction or desorption. Due to ultrafast electronic relaxation, the nuclear motion proceeds via multiple potential surfaces. Thus, within the DIET framework, surface photochemistry can be broken down into three processes: excitation, relaxation, and wave packet propagation.

A. Excitation. Excitation of metals with light creates a near-surface nonthermal carrier distribution in a range of $-h\nu$ to $h\nu$ relative to the Fermi level E_F, as described in Figure 1a.[9,10,32−34] These "hot" electrons and holes evolve on a femtosecond time scale by carrier−carrier and carrier−phonon scattering, and transport.[35,36] In the standard scenario for DIET, the electronic excitation through the inelastic scattering of hot electrons into the unoccupied states of the adsorbate initiates the photochemistry.[10,11,31] However, DIET also can be initiated by direct optical excitation where an electron is excited within the adsorbate or from the substrate to the adsorbate.[33,34,37,38] Since electronic structure of the adsorbate is strongly perturbed by the metal substrate, it can be difficult to distinguish the direct excitation from the hot electron process. Often the main recourse for

* Corresponding author. Current address: Department of Physics and Astronomy, University of Pittsburgh, Pittsburgh, PA 15260. E-mail: petek@pitt.edu.

10.1021/jp0045235 CCC: $20.00
Published on Web 06/27/2001

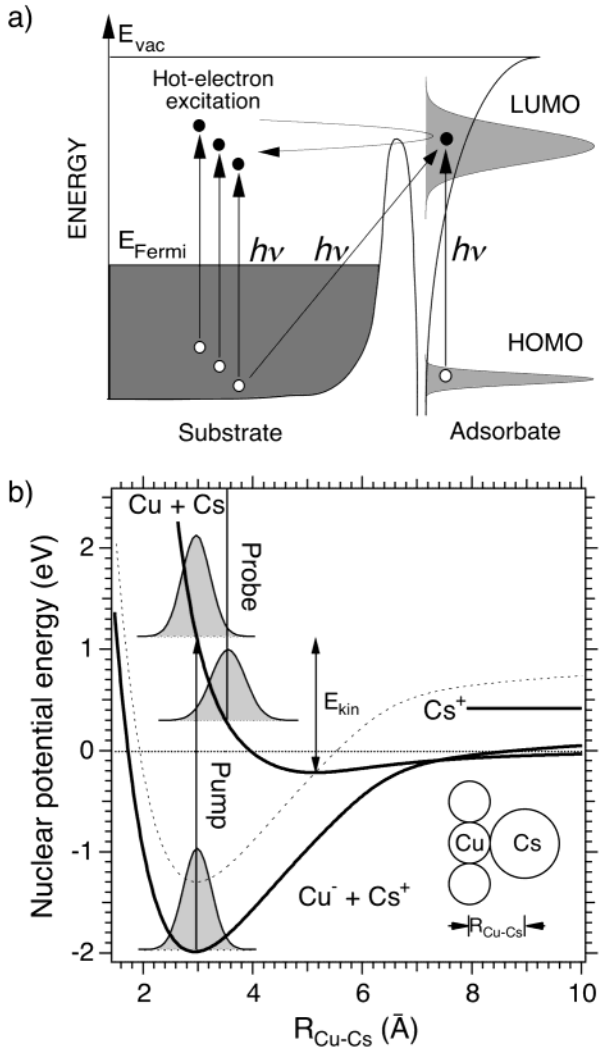

Figure 1. Schematic descriptions of the electronic and nuclear dynamics in surface photochemistry. (a) Electronic excitation of the unoccupied state of the adsorbate occurs either directly by optical excitation from the occupied states of the adsorbate or the substrate, or indirectly by hot electron generation in the bulk followed by the inelastic scattering with the adsorbate. (b) The empirical potential energy surfaces for photodesorption of Cs from Cu(111) are derived as described in the text. The asymptotic energies for Cs (defined as zero) and Cs^+ (horizontal line) depend on Θ_{Cs}. Franck−Condon transition to the excited state creates a wave packet, which propagates in response to repulsive forces in the excited state. Desorption can occur from the ground state when the wave packet has reached the critical propagation distance z_c where the kinetic energy acquired on the excited state exactly matches the Coulomb potential well depth of the ground state. A nonadiabatic transition is represented by the dashed line, which is just the ground-state potential displaced by $e-h$ energy that is transferred to the substrate. Desorption of neutral Cs atoms can occur only if the wave packet motion is entirely on the excited state or through multiple nonadiabatic transitions between the excited and ground states. This one-dimensional picture ignores the motion of substrate atoms (phonon generation) from the recoil of Cs atoms.

distinguishing between the direct and the hot electron mechanisms is the dependence of the reaction cross section on the polarization and frequency of the excitation light.[10,39−41] By contrast, two-photon photoemission spectroscopy directly probes the adsorbate excitation mechanism.[20,22,42]

B. Relaxation. Strong coupling between the adsorbate and substrate will induce rapid electronic relaxation in competition with DIET. Relaxation occurs both elastically by the delocalization of charge into the substrate following resonant charge

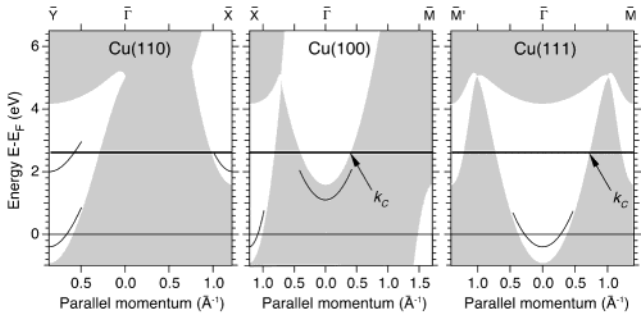

Figure 2. (a) Schematic of the experimental apparatus. Sample preparation and alkali atom deposition are performed in a dedicated UHV chamber that is attached to the photoemission chamber (not shown). Feedback control of the Mach−Zender interferometer is described in ref 53. (b) I2PC trace for the near resonant excitation of the Cs antibonding state from the occupied surface of Cu(111) that is calculated by optical Bloch equations for the indicated three-level system. In the simulation, all of the phase relaxation times are set to 15 fs, the population decay time is 50 fs, and the detuning of the laser from the resonance is 0.17 eV. The quantum beat-like oscillations in the I2PC results from the interference between the driving frequency of the excitation field, and the near resonantly excited polarization at 0.17 eV higher frequency.[24] The I2PC scan is decomposed into its component envelopes.

transfer (RCT), or inelastically by the electron−electron (e−e) scattering of adsorbate-localized electrons and the Fermi sea. Lifetimes can be deduced from photochemical yields and distributions based on simulation of the nuclear dynamics on model ground and excited-state potential energy surfaces (PES).[11,14,17,43] Alternatively, photoemission line widths of unoccupied states also provide lower limits for lifetimes of typically ≪10 fs through the Heisenberg uncertainty relation $\Gamma\tau = \hbar$.[18,44−50] However, since line widths can also have unknown contributions from inhomogeneous sources or from elastic carrier scattering,[49] time-resolved methods should be able to provide the most direct measurement of the true lifetimes.[51] Time-domain measurements on Cs/Cu(111) described here provide a vivid example where the directly measured lifetimes are significantly longer than those implied by the line widths.[22]

C. Desorption. Electronic excitation induces forces that lead to the nuclear wave packet motion on the excited PES. These forces may be attractive (Antoniewicz)[30] or repulsive (Menzel−Gomer−Redhead (MGR))[28,29] propelling the nuclear wave packet into or away from the surface, whereby the adsorbate acquires kinetic energy. A nonadiabatic transition projects the displaced wave packet down to the ground PES, as shown for the MGR scenario in Figure 1b. When the transition occurs past a critical internuclear distance z_c, the adsorbate will have gained sufficient kinetic energy to desorb on the ground PES.[14,17] The MGR model is the appropriate starting point for discussing the photodesorption dynamics of alkali atoms from copper.[26,52]

D. Interaction of Alkali Atoms with Metal Surfaces. The chemisorption of alkali atoms on metals introduced in this subsection provides the context for interpreting the spectroscopic and dynamical results.

1. Electronic Structure. The electronic excitation of alkali atoms by photoinduced charge transfer and relaxation by the reverse charge transfer into the bulk are determined by the band structure of the substrate and the local electronic properties of the chemisorption bond.[53] In Figure 2, the band structures of the low-index surfaces copper for momentum component parallel to the surface $k_{||}$, show that for the Cu(111) and Cu(100) there exist projected band gaps for a range of momenta about $k_{||} = 0$. At $k_{||} = 0$ these band gaps extend respectively

from −0.85 to 4.2 eV and from 1.6 to 8 eV (all energies are given with respect to E_F).[54] These band gaps exclude propagating Bloch states in the bulk for a range of momenta about the surface normal. Furthermore, surface states that are bound by the image potential, as well as free electron waves propagating in vacuum that can be excited above the work function (so-called "inverse LEED" states), have only evanescent amplitudes in the bulk.[55] By contrast, for Cu(110) there is no gap at $k_{||} = 0$ for unoccupied states of relevance to the present experiment (<6.2 eV).[56] Moreover, at the metal−vacuum interface there exist a partially occupied surface state (SS) for Cu(111) at −0.39 eV and other occupied and unoccupied states and resonances that are indicated in Figure 2.[48,57] Projected band gaps localize wave functions in the near surface region for the SS and other surface states, while the hybridization with the resonant Bloch waves leads to delocalized bands for resonances. Thus, the band gaps define the phase space for confinement of electrons to the surface.[49,58]

2. Alkali Atom Chemisorption. The appropriate description of the alkali atom chemisorption in the context of ionic or covalent bonding is subject of debate.[59−68] Here, the object is to present the surface electronic structure and potential energy surfaces for the alkali atom chemisorption that is consistent with the ITR-2PP measurements.

As the alkali atom approaches a metal surface, the positive ionic core of the alkali atom induces a negative image charge in the metal. Consequently, the Coulomb repulsion between the highest occupied ns electron of the alkali atom and the core-induced charge density in the metal destabilizes the ns electron with respect to E_F. This makes charge transfer into the unoccupied states of the metal energetically favorable and therefore, the ns resonance broadens corresponding to the rate of the electron transfer between the surface.[58,62,69,70] Delocalization of the ns electron into the substrate provides the driving force for the formation of the chemisorption bond.

Chemisorption of alkali atoms induces characteristic changes in the surface density of states (DOS).[59−67,71−75] The DOS associated with the ns resonance has yet to be fully described by photoemission spectroscopy, the primary method for studying chemisorption. The ns resonance is difficult to observe because of both a small cross section for photoemission of s electrons and its large bandwidth. It has been observed only by He metastable deexcitation and inverse photoemission (IPE) spectroscopies, which find a broad (∼3 eV) resonance straddling E_F.[72,76,77] For several alkali atoms and substrates, IPE and 2PP spectra reveal another resonance at ∼3 eV (zero alkali atom coverage limit) having a much narrower (≪1 eV) width.[76−80]

The partially covalent description of the alkali atom to metal surface bond provides a useful framework for understanding the chemisorption and the photoexcitation process.[63−65] The interaction of a highly polarizable alkali atom with a metal surface induces intraatomic hybridization.[61] The DOS associated with the alkali chemisorption has some character of intraatomic ns−np_z hybridization, where the electron density is displaced from the alkali atom core to the metal surface.[64,65,75] However, above E_F the polarization of charge reverses to ns + np_z antibonding character where the charge is displaced to the vacuum side of the alkali atom.[81] The DOS associated with this state has a maximum at ∼3 eV, and thus, most likely corresponds to the unoccupied resonance in IPE and 2PP spectra.[65] Significantly, the calculated transition moment for the optical excitation between the bonding and antibonding state is large.[81] Thus, the photoexcitation to the antibonding state substantially changes the surface charge distribution, which can be viewed as either a reverse charge transfer, whereby an electron from the metal neutralizes the alkali atom, or more descriptively, as a displacement of charge from the chemisorption bond to the vacuum side of the alkali atom. This change in the electronic environment of Cs atoms turns on the Coulomb repulsion, and thereby initiates the dissociative wave packet motion.

The above scenario can be represented by schematic potential energy surfaces in Figure 1b. The PESs are based on the above description of the alkali chemisorption and previous studies of photodesorption from graphite and oxide surfaces.[52,75,82,83] The relative asymptotic energies of the alkali atom and its cation are given by the energy required for transferring an electron from a free Cs atom with an ionization potential $IP = 3.9$ eV to the Fermi level of Cu(111), i.e. $IP - \Phi$, where Φ is the work function of the substrate. Θ_{Cs} determines Φ and the Cs−Cs interaction, and thereby, some features of the potential energy surfaces such as the asymptotic energies, the chemisorption bond strength, and whether and at what distance the ionic and neutral surfaces cross. The potential curves in Figure 1b are for typical $\Theta_{Cs} = 0.1$ ML used in the 2PP experiments. The binding energy of a neutral Cs atom is estimated from temperature programmed desorption measurements on Cs/Ag(100).[84] The ionic potential is constructed by splicing a long-range Coulomb potential corresponding to $\Phi = 3.8$ eV to a short-range Morse potential described by a well depth of 1.9 eV[84] and equilibrium bond length of 2.97 Å from theory.[58] The neutral surface is constructed with a long-range van der Waals potential,[85] and a short-range exponential repulsion that gives the observed excitation energy of the antibonding state at 2.6 eV.

III. ITR-2PP Experimental Technique

A time-resolved photoemission experiment is performed with a sequence of typically <100 fs laser pulses that excite and test the time evolution of the near-surface carriers. The electronic and nuclear dynamics are monitored by measuring energy and momentum resolved photoemission current induced by the pump−probe excitation. Photoelectrons carry the spectroscopic and dynamical information on the initial, intermediate, and final states in the two-photon excitation process.[53]

A. Experimental Apparatus. A schematic of the ITR-2PP apparatus is shown in Figure 3. A more comprehensive description of the ITR-2PP method is published in ref 53. The apparatus consists of the ultrafast laser for excitation, the Mach−Zender interferometer (MZI), for the pump−probe delay generation, and the ultrahigh vacuum (UHV) system for the 2PP measurements.

The excitation light is produced with a Ti:sapphire laser oscillator operating at 800 nm, having 500 mW average power, and 80 MHz repetition rate. Its output is converted with ∼20% conversion efficiency to the second harmonic at 400 nm (3.08 eV) in an 80 μm thick β-BaB_2O_4 (BBO) nonlinear crystal. The passage of the 400 nm light through the MZI generates identical pump−probe pulses with a well-defined delay Δ. Before entering the UHV chamber, the polarization with respect to the optical plane, which is defined by the reflection from the sample surface, is set with a $\lambda/2$ plate. Prism-pair sequences compensate for the group-velocity dispersion in the optical system for both the 800 and 400 nm light in order to achieve minimum pulse widths at the BBO crystal and the sample. Temporal widths of both the 800 and 400 nm pulses at the sample are determined to be 19 ± 1 fs by interferometric autocorrelation measurement of second harmonic generation from the Cu(111) surface.[86] Precise characterization of the excitation pulse at the point of the 2PP measurement is a prerequisite for accurate determination of the carrier relaxation processes.[86,87]

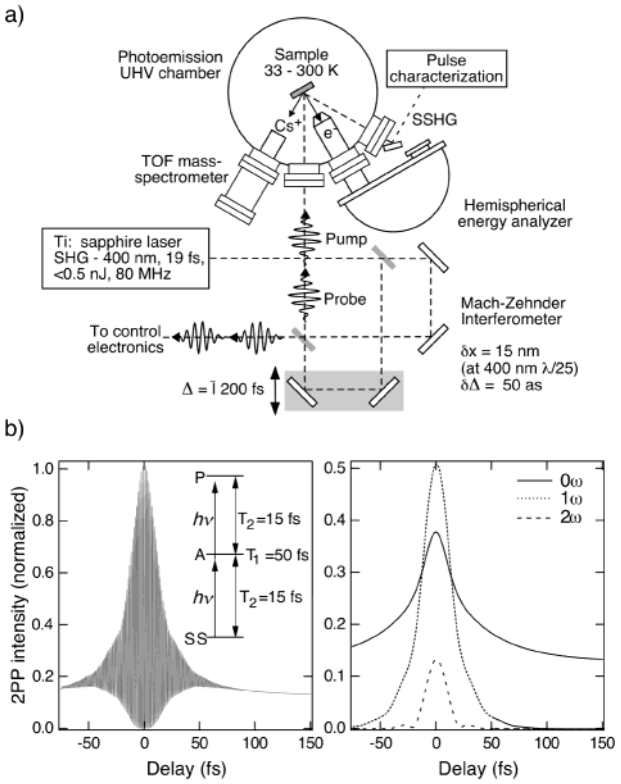

Figure 3. Band structure of copper for the surface parallel momentum. Shaded regions represent 3D propagating Bloch states, and white areas the projected band gaps. Known low energy surface states are indicated by black curves. The thick solid line represents the dispersionless Cs antibonding state at an energy appropriate for the experiments on Cu(111). The resonant SS → A transition energy is tuned by controlling Θ_{Cs}.

The UHV photoemission chamber is made of μ-metal and has a base pressure of $<5 \times 10^{-11}$ Torr. 2PP signal normal to the surface is recorded with a Vacuum Generators 100AX hemispherical electron energy analyzer, with specified energy and angular (momentum) resolution of 100 meV and 5°. Actual energy resolution of $\leq$ 28 meV, as determined from the width of the Φ cutoff in the 2PP spectra, is achieved by minimizing stray magnetic fields and improving the stability of the control electronics. The instrumental resolution of 80 meV, as deduced from the Fermi edge of copper, is dominated by the frequency spread of the ultrafast laser pulse. The laser is incident 30° from the analyzer axis and is brought to 80−100 μm diameter focus on the sample.

The Cu(111), (100), and (110) samples are prepared by a standard cyclical procedure of sputtering and annealing in an attached MBE chamber (not shown).[53] After depositing at 300 K, a fraction of a monolayer ML of Cs from a SAES getter source, the samples are transferred under UHV conditions into the photoemission chamber. (For Cs/Cu(111), the coverage $\Theta_{Cs} = 1$ ML is defined by the p(2 × 2) structure with a surface density of 4.41×10^{14} atoms/cm^2, and is determined from the published dependence of Φ on Θ_{Cs}.[79]) Sample temperatures in the range of 33−300 K are set by a He closed-cycle refrigerator/heater combination.

Two main modes of performing the experiments consist of measuring the 2PP spectra and interferometric two-pulse correlations (I2PC). 2PP spectra are recorded by accumulating the photoelectron counts for a defined time interval as the analyzer pass energy is scanned. The excitation can be induced by either a train of single pulses, or pump−probe pulse pairs, where Δ is fixed with an uncertainty of 50 as. For I2PC measurements, the analyzer is set to a specific energy and Δ is scanned continuously and repetitively by up to 300 fs with 1.77 Hz frequency. The delay scanning is synchronized with the data acquisition through a feedback control of the MZI, ensuring that in averaging repetitive scans (typically 400−2000) the scan-to-scan jitter in Δ is <50 as. This ensures that the quality of I2PC data is limited only by the electron counting statistics and the residual jitter in the interferometric scan reproducibility.

B. Data Reduction. Before proceeding to the results, it is important to introduce how the 2PP excitation process is recorded in the I2PC scans. The 2PP excitation from Cs/Cu(111) can be approximated by a three-level scheme defined by SS, the antibonding state A, and the final state selected by the analyzer P (Figure 3b). The resonant frequencies for the SS → A and A → P transitions are adjusted by Θ_{Cs} and the pass energy of the analyzer to be nearly equal to the excitation frequency. Near-resonant laser excitation creates coherent polarization components that oscillate at the resonant frequencies, as well as the population in the intermediate state A. The time-integrated population of P as a function of Δ, which is recorded in the I2PC scans, reflects the polarization and population dynamics in the sample.[53,87]

The excitation of this three-level system can be described by optical Bloch equations (OBE), as discussed in ref 87. Figure 3b shows a simulated I2PC scan calculated with OBE using phase and energy decay parameters that are appropriate for Cs/Cu(111).[22,26] The I2PC scans include rapidly oscillating components at approximately the laser frequency and its second harmonic, and a slower decay of the intermediate state population. The oscillations arise from the interference between the pump and probe excitation fields and the coherent polarizations that they excite in the sample. I2PC scans can be analyzed into component envelopes of oscillations at the excitation frequency 1ω, and its second harmonic 2ω, and slowly varying envelope 0ω consisting of an average over the phase of 1ω and 2ω oscillations. The latter is identical to a more commonly measured noncollinear two-pulse correlation, where the distinction between coherent and incoherent components is lost by averaging over the optical phase.[53,88] However, in an interferometric measurement these can be separated, because the former contributes to the 1ω and 2ω envelopes, whereas the latter contributes only to the 0ω envelope. Thus, after analyzing the coherent polarization dynamics from the 1ω envelopes, the population dynamics can be evaluated unambiguously from the 0ω envelopes. Furthermore, for an asymmetric three-level system ($E_A - E_{SS} \neq E_A - E_P$), the laser excites coherent polarizations with oscillation frequencies defined by $(E_A - E_{SS})/\hbar$ and $(E_P - E_A)/\hbar$, and decay rates $\Gamma_{SS,A}$ and $\Gamma_{A,P}$. Interference among the coherent polarizations and the near resonant driving field results in the characteristic beating in the 1ω envelopes that appears in Figure 3b.[24]

IV. Results and Analysis

A. 2PP Spectra. Whether the photoexcitation of the antibonding state occurs indirectly through the hot electron mechanism, as proposed for the photodesorption of K from graphite (K/C),[52] or directly from the occupied states of the alkali atom or the substrate can be established from the systematic changes in the 2PP spectra when Θ_{Cs} is sequentially increased. The 2PP spectrum for $k_{||}$ and $\Theta_{Cs} = 0$ in Figure 4 shows a single peak due to coherent two-photon excitation from SS at 5.8 eV on top of a continuous pedestal representing momentum integrated emission from the bulk bands. Adsorption of Cs introduces a new resonance, which is attributed to A.[21,77,80] Increasing Θ_{Cs}

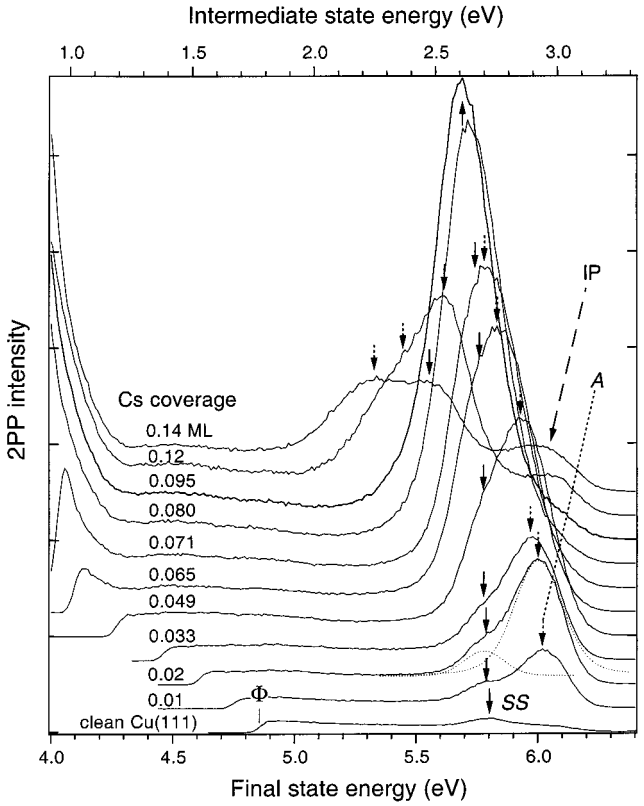

Figure 4. Θ_{Cs} dependence of 2PP spectra of Cs/Cu(111) at 300 K, which show the resonance enhancement of the SS → A transition. The arrows indicate approximate positions of SS, A, and at highest Θ_{Cs}, IP states. Dotted curves indicate the Voigt line shape deconvolution of the SS and A peaks.

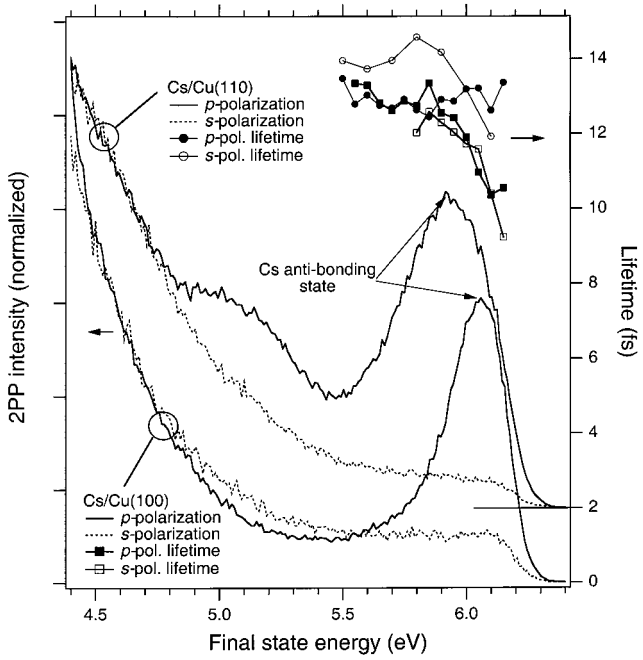

Figure 5. 2PP spectra and population decay times for Cs/Cu(100) and Cs/Cu(110) that are taken with s- and p-polarized excitation at 33 K. The spectra are normalized at 4.7 eV. The additional feature in the p-polarized spectrum of Cs/Cu(110) is probably due to the intrinsic unoccupied surface state (see Figure 3). The lifetimes with s- and p-polarized excitation (squares and circles) are the same, indicating that the resonant charge transfer is faster than the hot electron decay.

up to 0.5 ML decreases the vacuum level,[79] which changes the image potential and, therefore, the conditions for the confinement of SS and A at the surface. Since A is closer to the vacuum level than SS, the increasing width of the confining potential decreases the energy of A more than for SS, and therefore, the energy required for the SS → A excitation also decreases with Θ_{Cs}. The resonance with the 3.08 eV excitation light occurs for $\Theta_{Cs} \approx 0.095$, where in Figure 4 the SS and A peaks coalesce and reach maximum integrated intensity. Two distinct peaks reappear at even higher Θ_{Cs}, but with a reduced integrated intensity. *This resonance enhancement of the SS → A transition constitutes the frequency-domain evidence for direct surface-to-adsorbate excitation.*

Other changes in the 2PP spectra of Cs/Cu(111) with temperature and time, which have been noted in ref 22, also may be relevant to the photodesorption dynamics. Upon cooling, Φ, A, and SS tune linearly with respective rates of +0.28, +0.19, and −0.18 meV/K.[22] Similar spectral shifts also occur at constant temperature in the dark, but the rate of increase is larger when the sample is irradiated by 3.08 eV light. These changes imply a decrease in the Cs concentration, which could result from thermal diffusion of Cs atoms[89] and photodesorption.

The unique electronic properties of Cs/Cu(111) are manifest when its spectroscopy and dynamics are contrasted with those of the other low index surfaces of copper. Figure 5 shows the 2PP spectra of Cs/Cu(100) and (110) at 33 K for $\Theta_{Cs} \sim 0.04$ ML, where the corresponding Cs antibonding states appear as resonances at 2.98 and 2.85 eV. Although, the 2PP spectra of these surfaces do not reveal a clear signature the initial state for the excitation of A, the photoinduced charge-transfer excitation could occur from the 6s-6p_z bonding DOS of Cs, or the sp band of the substrate. Although the characteristic resonant behavior as observed for Cs/Cu(111) is not expected for the excitation from these broad bands, the I2PC measurements to be introduced later do favor the direct over the hot-electron excitation mechanism. A further point of contrast are the Lorentzian line shapes Γ^A, which at 33 K are 70, 250, and 300 meV for Cu(111), Cu(100), and Cu(110),[22] implying minimum excited-state lifetimes of 9.4, 2.6, and 2.2 fs, respectively. The origin of this crystal face dependence of Γ_A will be discussed in section V.

B. Interferometric Two-Pulse Correlation Measurements. The interferometric two-pulse correlation measurements probe the electronic and nuclear dynamics that are initiated by excitation of the Cs antibonding state. Figure 6 presents 2PP spectra for $\Theta_{Cs} = 0.10$ ML taken at 33 K with both s- and p-polarized excitation, and I2PC traces taken near the SS → A resonance with p-polarized excitation. Figure 7 shows the analysis of the I2PC scans into the 0ω and 1ω envelopes (the 2ω envelopes are not discussed since the nonlinear polarization couples only SS and P[88,90]).

1. Coherent Antibonding State Excitation. The s- and p-polarized measurements provide the basis for discussing the excitation and relaxation mechanisms of A on the low index surfaces of copper. By contrast to p-polarization, the s-polarized 2PP spectra and I2PC envelopes in Figures 6 and 7 show neither the SS → A resonance nor the accompanying envelope broadening. Due to the fact that, because of symmetry, the p-polarization probes mainly the antibonding state whereas the s-polarization probes only the bulk hot electrons, this data set contrasts the surface and bulk dynamics.

The comparison of 1ω envelopes with different polarizations in Figure 7a shows that the most pronounced broadening occurs at energies where A dominates the 2PP spectrum. Because s-polarization couples continuous bands that give a flat 2PP spectral distribution characterized by large inhomogeneous broadening, the 1ω envelopes reproduce the width of the laser

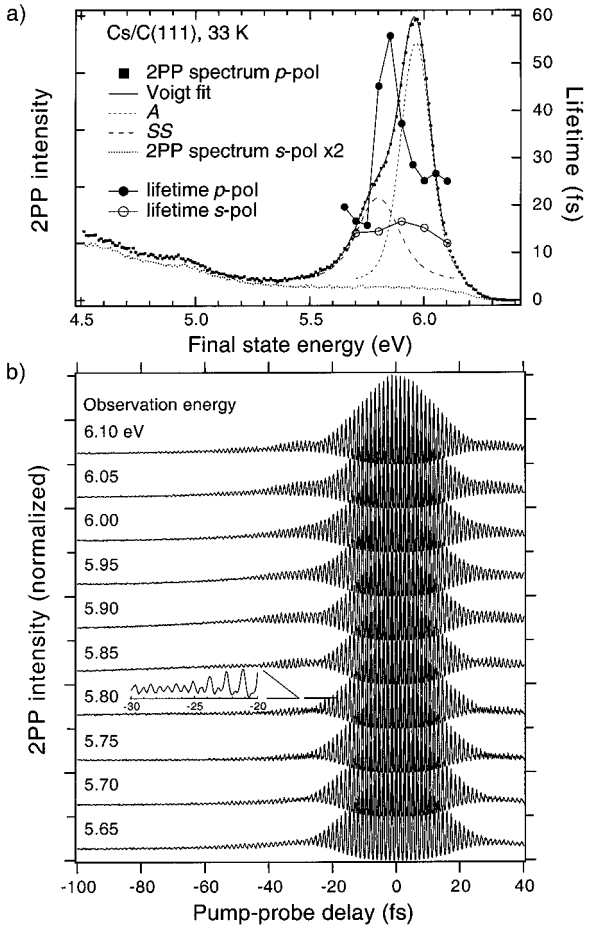

Figure 6. (a) The 2PP spectra and population decay times for Cs/Cu(111) that are taken with s- and p-polarized excitation at 33 K. Solid and dashed lines show a Voigt line shape deconvolution of SS and A. (b) I2PC scans for p-polarized excitation from which the phase and population dynamics are deduced. Interference between the polarization waves excited in the sample produce the coherent oscillations at approximately the excitation frequency and its second harmonic (see inset).

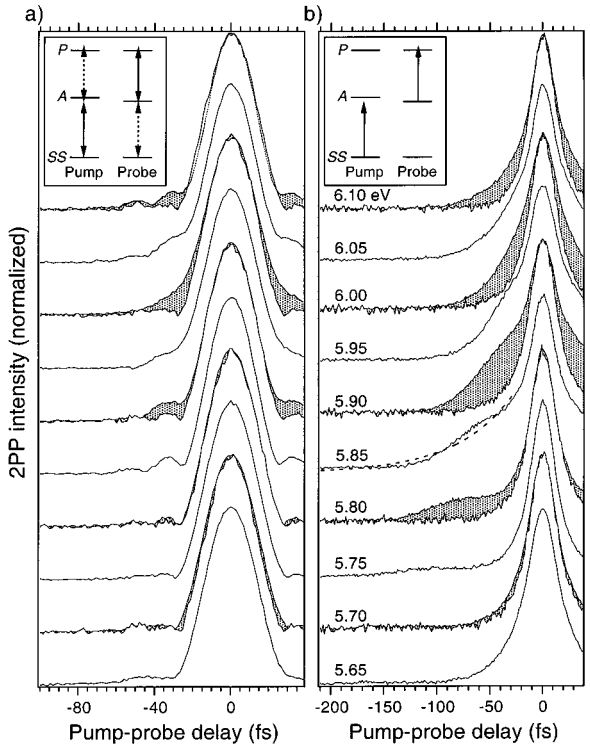

Figure 7. (a) 1ω and (b) 0ω envelopes from I2PC scans for s- and p-polarized (shaded; from data in Figure 6) excitation. Insets show the particular (a) linear polarization, and (b) population dynamics measured by each component envelope. The dashed line shows a forced exponential fit to emphasize the nonexponential nature of the population dynamics. The data in Figure 6a are obtained from such fits and should be taken only as effective parameters from an oversimplified fitting model.

pulse.[87] The additional width observed at the SS $\rightarrow$ A resonance with the p-polarization indicates that the 3.08 eV light excites a coherence between SS and A, which decays with a finite phase relaxation time that can be deduced from the analysis of 1ω envelopes. This direct coupling of SS and A further substantiates that the excitation proceeds *coherently* through photoinduced charge transfer.

The phase relaxation of *A* can be evaluated unambiguously in experiments under near-resonant excitation, where the SS and A peaks are partially resolved.[22,23] Under these conditions, at observation energies corresponding to the top of the antibonding state peak, the 1ω oscillations are dominated by the coherent polarization induced by the A $\rightarrow$ P transition. The phase relaxation rate $(\Gamma^{AP})^{-1}$ fs is obtained by fitting the 1ω envelope. Assuming that $\Gamma^{AP} = \Gamma^{A} + \Gamma^{P}$, i.e., the decoherence rate is the sum of scattering rates of uncorrelated particles,[47,91] and that $\Gamma^{P} \approx 0$ leads to conclusion that $(\Gamma^{A})^{-1} \approx 15$ fs. The latter assumption is justified since 2PP excitation couples the surface states to inverse LEED final states, which have a negligible scattering probability.[92] The time-domain measurement of Γ^{A} is to be compared with the Lorentzian width of *A*, which implies a phase relaxation time $T_2 = 19 \pm 3$ fs. The correspondence between the time- and frequency-domain values of Γ^{A} is consistent with a predominantly homogeneous broadening mechanism.[22]

I2PC measurements are also performed on Cs/Cu(100) and Cu(110) in order to determine the excitation mechanism and lifetime of the corresponding antibonding states. Similar conclusions cannot be made regarding the excitation mechanism as for Cs/Cu(111), because 1ω envelopes are the same at the observation energy of A for both the s- and p-polarized excitation due to the rapid decoherence. However, I2PC scans can distinguish between predominant excitation of A via the hot electron vs the direct optical excitation mechanism through the analysis of the ratio of the coherent component to the I2PC baseline.[93] In the hot electron scenario the probability of excitation to A is determined by the transition moment for creating hot electrons scaled by the probability of hot electrons scattering into A. Substantial contribution of excitation through this indirect path would attenuate the coherent-to-baseline intensity ratios.[93] However, the observed ratios for Cs/Cu(100) and (110) are consistent with predominantly direct excitation. This is to be expected because A dominates the high-energy region of the 2PP spectra, and no large source of hot electrons exists at higher energies that could scatter into A.

2. Cs Antibonding State Relaxation. The I2PC scans also provide information on the electronic relaxation of A. Figure 7b contrasts several 0ω envelopes taken with the s- and p-polarization near the SS $\rightarrow$ A resonance, where the former probes the population relaxation of hot electrons in the bulk, while the latter probes the population dynamics of A. In the energy range where A dominates the 2PP spectrum, the average lifetime of hot electrons is $\sim$14 fs, which is comparable to that of clean copper surfaces.[94] By contrast, the excitation of A results in considerably longer and highly *nonexponential*

TABLE 1: Measured Lifetimes and Photoemission Linewidths of Alkali Atom Antibonding States on Metal Surfaces[a]

				theory			
surface	temp (K)	lifetime (fs)	line width (meV)	Γ_{RCT} (meV)	Γ_{e-e} (meV)	bond length (Å)	adsorption site
Cs/Cu(111)	33	~50[b,c]	70 ± 10	7	16.5	3.08[96]	atop
	300	12 ± 2	350 ± 50				
Rb/Cu(111)	33	~25[25,b]				3.07[97]	atop
Na/Cu(111)	300	(1.6)	410 ± 30[79]				
Cs/Ag(111)	33	~30[b]				3.02 ± 0.03[98]	fcc hollow
	300	>7	<420[21]				
Cs/Cu(100)	33	(2.6)[b]	250 ± 20	20	112	2.94[99]	hollow
	300	6 ± 4	400 ± 50[21]				
Na/Cu(100)	300	<4	520 ± 50[21]			2.23[100]	hollow
Cs/Cu(110)	33	(2.2)[b]	<300				
K/graphite	83	50[52]					

[a] The implied lower limits of lifetimes from the linewidths are given in parenthesis. The bond lengths and adsorption sites from structural analyses are given where measured. [b] Present work. [c] The observed decay is nonexponential.

population dynamics. Because it is difficult to quantify the decay times by a more appropriate means, Figure 6a presents the effective "lifetimes" derived by forcing exponential fits to data in Figure 7b. These nonexponential decays can result from interplay of electronic relaxation and unusual excited-state population dynamics due to the nuclear wave packet evolution, as will be discussed in section V.

The population and polarization decays probed by the 0ω and 1ω envelopes in Figure 7 occur on clearly different time scales. This subverts the commonly invoked ansatz equating the reciprocal photoemission line widths with the quasiparticle lifetimes.[47,95,96] The homogeneous line width is proportional to the phase relaxation rate and can be expressed as a sum of, respectively, the inelastic (population) and elastic (pure dephasing) contributions $\Gamma^A = 1/2\Gamma^A_{\text{inelastic}} + \Gamma^A_{\text{elastic}}$. Since the population decay rate of $\Gamma^A_{\text{elastic}}$ 50^{-1} fs^{-1} is significantly slower than the phase relaxation rate of 15^{-1} fs^{-1}, the pure dephasing is the *dominant* contribution to Γ^A_{tot}. The previously reported temperature dependence of both the population and phase relaxation rates suggests that phonons play an important part in both.[22] The electron−phonon scattering contribution to the phase relaxation rates of the intrinsic surface[48,49] and bulk[50] bands of copper is well established. The effect is considerably larger for the Cs/Cu(111) surface, suggesting that the Cu−Cs vibrations may be more effective in inducing phase relaxation than the substrate phonons.

Before proceeding to the discussion of the nonexponential behavior in the population dynamics, it is interesting to contrast Cs/Cu(111) with the other low-index surfaces of copper. Figure 5 presents the exponential decay times for the Cs/Cu(100) and Cs/Cu(110) surfaces near the SS → A resonance. By contrast to Cs/Cu(111), the lifetimes are on the average 12−13 fs independent of the s- or p-polarization. Although A dominates the p-polarized 2PP spectra, the population dynamics are the same as for the hot electrons of the same energy. This dramatic band structure effect will be discussed in section V.

V. Discussion

The direct time domain observation of the phase and energy relaxation of an electronically excited adsorbate on a metal surface provides new insights into the excitation, relaxation, and wave packet propagation in DIET.

A. Excitation Mechanism. The mechanism for the photoexcitation of adsorbates on metal surfaces is an important issue in the field of surface photochemistry. Most photochemical studies, with a few exceptions, favor the hot electron mechanism.[10,32,34,52] However, while the hot electron dynamics in metals is the subject of several ultrafast TR-2PP experiments, none provide time-domain evidence for significant adsorbate excitation via the hot electron mechanism.[53] Here, both the 2PP spectra and I2PC measurements demonstrate that Cs atoms are excited through the direct optical excitation. This conclusion is also supported by the polarization dependence of 2PP spectra: Bauer et al. demonstrate for Cs/Cu(111) that A cannot be excited with s-polarization, excluding the hot electron mechanism.[20,21,97] The direct excitation process also predominates for CO/Cu(111), where the polarization dependence of 2PP spectra suggests the direct mechanism for all but the lowest lying unoccupied state, where the hot electron density is the highest.[42] Unfortunately, no system with well-characterized hot electron-induced photochemistry has also been investigated by TR-2PP.

B. Alkali Atom Antibonding State Lifetimes. The ITR-2PP measurements show a remarkable dependence of excited-state lifetime τ_A on the crystal face. Table 1 compiles values of τ_A for alkali atoms on a variety of metal surfaces for the purpose of discussing factors that might affect electronic relaxation rates of adsorbates on metals. These lifetimes probably have contributions from both the elastic surface-to-bulk resonant charge transfer (RCT) and inelastic decay through e−e scattering.[22,26,98,99]

On one extreme, the estimated lower limits for the lifetimes for Cs/Cu(100), Cs/Cu(110), and Na/Cu(100) from Γ^A_{exp} are on the order of few femtoseconds, which is typical of reported lifetimes from photodesorption cross sections of molecules,[10,12,13] and for RCT from the potassium-like core excited Ar atoms.[74,100] Because these implied values of τ_A are considerably smaller than for the isoenergetic hot electrons in the bulk, e−e scattering probably makes only a minor contribution to the overall electronic relaxation.[98] Rather, Γ^A_{exp} probably represents the RCT rate whereby the localized electron on the Cs atom decays into a delocalized state formed by the hybridization of *A* with the 3D propagating Bloch states of the metal. This scenario is confirmed by Borisov et al., who calculate that Γ^A_{exp} for Cs/Cu(100) has 85% contribution from the RCT process (see Table 1).[98] Since for the Cu(100) and Cu(110) surfaces the laser pulse is longer than $(\Gamma^A_{\text{exp}})^{-1}$, the excitation creates a delocalized state, and therefore, the measured values of τ_A are those of the bulk hot electrons.[101]

On the other extreme, Table 1 shows that τ_A for Cs/Cu(111) is at least an order of magnitude longer than for the (100) or (110) surfaces. Although τ_A for Cs/Cu(111) is unusual, similar though less exceptional results are obtained when Cs is replaced by Rb, or for (111) surfaces of other noble metals.[25] For (111) surfaces, the electron is localized on the alkali atom since τ_A is

considerably longer than for the isoenergetic bulk electrons. Borisov et al. show that the electronic relaxation occurs predominantly through e−e scattering, but less effectively than in the bulk, because of small overlap between charge densities of the antibonding state and the substrate.[58,98,102]

The inhibited electronic relaxation of alkali atoms appears to follow from a singular aspect of the (111) surfaces of noble metals, namely the location of the antibonding state in the projected band gap.[22,58,103] It is now well established that *dispersive* surface states such as the image potential states on the (111) and (100) surfaces of noble metals can have lifetimes extending into the picosecond range. For states with defined $k_{||}$, the band gap defines the range of $E(k_{||})$ where the surface wave functions cannot propagate in the bulk.[49,104−106] Since under present experimental conditions Cs atoms form a disordered layer, A is *localized* on individual adsorbates. RCT can in principle occur to all nearly isoenergetic states outside of the projected band gap (charge transfer must occur to lower energy bulk states because of the possible vibrational excitation of the adsorbate and electromagnetic emission associated with an accelerating charge),[107,108] because for a localized state, $k_{||}$ is undefined.

However, according to Borisov et al., even if the elastic decay is not inhibited by momentum conservation, the projected band gap can still inhibit RCT. The band gap prevents RCT from occurring only for finite values of parallel momentum less than k_c, the minimum momentum for 3D propagating bulk bands. However, entering the bulk with a large parallel momentum is unfavorable because the barrier width for tunneling increases with the angle from the surface normal.[58,98,99] Although propensity for the lifetime to scale with k_c is consistent with the observed electronic quenching rates of alkali atoms on the (111) surfaces of noble metals, the precise role of the projected band gap is still not clear. Even though the antibonding state at $k_{||} = 0$ is resonant with the band gap for Cs/Cu(100), but not for Cs/Cu(110), their Γ^A_{exp} are comparable, implying that for Cu(100) the band gap does not impose a significant barrier to RCT. It is not clear whether the difference between Γ^A_{exp} for Cs/Cu(111) and Cs/Cu(100) arises mainly from different magnitudes of k_c, or if additional factors also strongly affect the RCT rates.

Table 1 shows that τ_A also depends on the nature of the alkali atom, the surface temperature, and the nature of the substrate. Bauer et al. argue that in addition to the distance of resonant bulk bands from the center of the surface Brillouin zone, the antibonding hybridization also affects τ_A.[21] The antibonding hybridization is related to the polarizability, and therefore, the energy gap between the ns and np orbitals of the free alkali atom.[25,109] Thus, considering their size and polarizability, the electron density of Cs atoms should be displaced furthest into vacuum. Moreover, Borisov. et al. argue that the polarization of the charge cloud normal to the surface also accentuates the propensity for the attenuation of RCT into off-normal directions.[98,99] Thus, the polarizability of alkali atoms can account for the observed trend in τ_A for Rb and Cs/Cu(111), or in Γ^A_{exp} for Na and Cs/Cu(100).

Surface temperature also has a pronounced effect on the energy and width of the antibonding state peak and τ_A, as reported in ref 22. Increasing temperature favors excitation of both the normal and lateral motion of Cs atoms. Excitation of the normal vibration affects both the average and extremal values of the bond length R_{Cu-Cs}, which could have a strong effect on the RCT rate, since in the case of free-electron metals, it increases exponentially with the distance of the adsorbate above the metal surface.[69,99] The situation may be more complex for Cs/Cu(111), because the calculated RCT rate is a nonmonotonic function of R_{Cu-Cs}.[58] However, the decrease of the antibonding state energy with temperature in 2PP spectra is consistent with an increase in the average Cu−Cs bond length, which decreases Coulomb interaction of Cs atoms with the surface.[22] Excitation of the lateral motion can affect the occupation of alkali atoms in atop or hollow sites, which may affect the coupling to the substrate.[22] However, since the lateral mobility of Cs atoms appears to be influenced more by the Cs−Cs repulsion rather than the surface corrugation,[110,111] at higher temperatures, Cs atoms will experience an increasingly inhomogeneous electronic environment due to local fluctuations in the Cs atom density, which may perturb the *z*-axis symmetry of the antibonding state electron density, and therefore, promote off-normal RCT.

Another factor that may promote the off-normal RCT is the alkali atom-induced rumpling of the surface. LEED structures of Cs/Cu(111) at one monolayer coverage find Cs atoms in the atop site with 0.12 Å buckling of the nearest Cu atom, while for Cs/Ag(111), Cs atoms are in the 3-fold hollow site and the substrate is considerably more rumpled.[112,113] Such specific interactions modify the local electronic environment of the alkali atoms, and thus might contribute to the modest difference in τ_A for Cs/Cu(111) and Cs/Ag(111), as well as to the crystal face dependence for copper. More significant alkali-atom induced local distortion of the surface on higher free energy surfaces such as Cu(100) may also enhance the rates.

C. Origin of the Nonexponential Decays. Before addressing the unusual nonexponential antibonding state dynamics in terms of the Cs atom desorptive motion, it is useful to summarize some distinct features and to exclude other possible scenarios. At low temperatures (<100 K) the population dynamics of A, as recorded by I2PC scans, are distinctly nonexponential. This effect is most pronounced when the SS → A transition is 0.1−0.2 eV *above* the excitation photon energy, and the observation energy is 0.1−0.2 eV *below A*. The effective decay rate appears to be a nonmonotonic function of time: in Figure 7b, at 5.80 eV the decay is fast for the first ∼50 fs and after ∼100 fs, but appears to decelerate between 50 and 100 fs. Such behavior is difficult to explain with simple kinetic schemes for the excitation migration and decay of randomly or inhomogeneously distributed particles in two dimensions.

Complex kinetics in a surface experiment could arise from inhomogeneities that are intrinsic to the surface or induced by adsorbates. Neither is likely for Cs/Cu(111) because (i) the dominant broadening of A at 33 K appears to be homogeneous and (ii) the decay of several distinct populations should lead to *multiexponential*, rather than nonexponential, kinetics. Inhomogeneous surfaces can result from surface reconstruction or island formation.[114] However, changes in the surface electronic structure as evidenced by Φ and E_A, the energy of A, are linear with temperature.[22] This is consistent with a phonon mechanism, rather than a structural phase transition, which should be more abrupt and, probably, irreversible.[67] Furthermore, the phase diagram for the observed structures of Cs/Cu(111) indicates only an orientationally ordered incommensurate phase at $\Theta_{Cs} < 0.12$ ML.[115] Moreover, He atom scattering studies of K and Cs/Cu(100) indicate isotropic alkali atom distributions down to 100 K, which also can be expected for the more stable and less corrugated Cu(111) surface.[110]

Adsorption of impurities such as water (or other commonly occurring, electron withdrawing species such as CO) also could produce an inhomogeneous surface. However, this would result in an abrupt change in Φ (up to −1 eV)[116] at the adsorption temperature (150 K for H_2O) with a sign opposite of that

observed. Moreover, complex kinetic processes such as the excitation migration and trapping at specific surface sites or by small polaron formation occur on significantly longer (>100 fs) time scales.[117−119] Thus, the nonexponential decays probably have a more fundamental origin.[22]

The nonexponential decays also could emanate from the specific electronic and nuclear changes set off by the SS → A excitation. Recall that the electronic excitation turns on the repulsive forces leading to the stretching of the Cu−Cs bond, as implied by Figure 1b, which, in case of potassium on graphite[52] and sodium and potassium on metal oxides,[82,83] leads to photodesorption. The stretching of Cu−Cs bond can affect I2PC scans through the dependence of the A → P transition moment, τ_A, or E_A on the internuclear distance R_{Cu-Cs}. The A → P transition moment strongly depends on R_{Cu-Cs}, because the excitation to the ionization continuum is only possible due to an abrupt change in the dielectric function at the surface.[120] Likewise, as already introduced above, τ_A is calculated to have nonmonotonic dependence on R_{Cu-Cs}.[58] Nevertheless, the most self-consistent explanation for the observed behavior is the monotonic decrease in E_A with R_{Cu-Cs}.[58,69] This correlation between E_A on R_{Cu-Cs} has already been invoked in the previous section to explain the temperature dependence of E_A. The most consistent explanation for the nonexponential population dynamics is the change in the SS → A and A → P transition energies stemming from the Cs atom motion.

D. Incipient Cs Photodesorption. The dependence of E_A on R_{Cu-Cs} implies that the surface electronic structure changes in response to the Cs atom nuclear motion. This change can be monitored with two-pulse excitation of 2PP spectra when the delay Δ is comparable to τ_A. Such spectra have a component where 2PP process is initiated by the pump pulse and completed by the probe pulse. Since different pulses induce the SS → A and A → P transitions, such spectra will detect a change in E_A and, therefore, the resonant transition energies during the interval Δ. However, the spectra also contain the usual Δ independent component where each pulse excites 2PP separately. To isolate the Δ dependent component, the independent component is recorded after A has decayed (pulse-pair delay of 240 fs) and subtracted from spectra taken with a shorter delay. Because for Δ < 80 fs the polarization decay is incomplete, delays are set precisely to $2\pi n$ multiples of the 1.34 fs optical cycle of the excitation light, to achieve constructive addition at the center frequency of the coherent polarizations excited by each pulse.[26,27] Since the energies of constructive and destructive interference depend on the phase, these measurements critically depend on the ability to maintain the relative phase for an arbitrary delay between the two pulses. Difference spectra showing the evolution of $E_A(\Delta)$ are presented in Figure 8.

Systematic changes in the difference spectra such as the decrease in E_A and experimental width of A, Γ^A_{exp}, provide the key for interpreting the Cs antibonding state dynamics. These changes are quantified by a Gaussian deconvolution of the SS and A peaks in each difference spectrum and the results are plotted in the inset of Figure 8. The second-order polynomial fit of $E_A(\Delta)$ indicates a *quadratic* dependence on Δ for both the E_A and Γ^A_{exp}. Before discussing the significance of these changes, note that with increasing Δ, the intensities of SS and the bulk hot electron background decrease relative to that of A. This is because the decay of the nonlinear polarization associated with SS and hot electron population decay faster[88,90] than the antibonding state.[94,121]

The quadratic change in Γ^A_{exp} arises from the interference between the pump and probe-induced polarizations known as

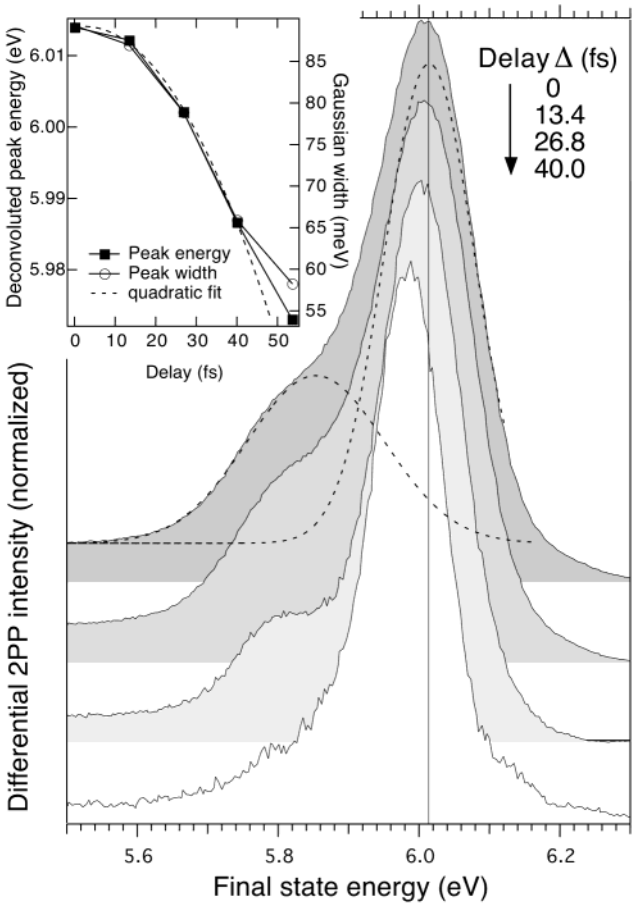

Figure 8. 2PP difference spectra that give snapshots of the nuclear wave packet motion in 13.4 fs, i.e., 10 optical cycle intervals. Dashed and solid vertical lines, respectively, show the deconvolution of the SS and A peaks, and E_A at zero delay. The inset shows the deconvoluted peak energy E_A and width Γ^A_{exp} vs the delay, as well as the second-order polynomial fit to the first four points of $E_A(\Delta)$.

optical Ramsey interference fringe effect.[122] This is the basis for the quantum control of the Cs atom motion as described in ref 27.

Here the focus is on the quadratic change of E_A with Δ. A spectral shift might arise from the many-body screening of the SS → A excitation by the low-frequency electron−hole fluctuations. However, such relaxation shift, if observable, would have an exponential dependence on Δ.[91] The observed quadratic dependence follows naturally from the most elementary model for the Cs atom desorption where the PES and the change in E_A with R_{Cu-Cs}, $E_A(R_{Cu-Cs})$ are approximated with negatively sloping linear functions. According to Newton's third law, the linear PES implies a constant force, and therefore, constant acceleration of Cs atoms, which yields a quadratic expression for $E_A(\Delta)$.

This model should explain not only the spectral changes but also the nonexponential decays. The effect of the Cs atom motion on the I2PC scans is simulated with an optical Bloch equation model for the 2PP process.[24] The excitation is described by a three-level scheme consisting of SS, A, and P, as shown in Figure 9, where the polarization and population decay times for A are set to 15 and 50 fs, respectively. The change in the surface electronic structure is modeled with $E_A(\Delta) = 2.7 - 0.12 \times 10^{-5} \times \Delta^2$, where the prefactor of Δ^2 is in units of eV·fs^{-2}. The comparison of the observed and calculated 0ω envelops in Figures 7b and 9 shows that the OBE simulation reproduces the nonexponential decays remarkably well. The main difference

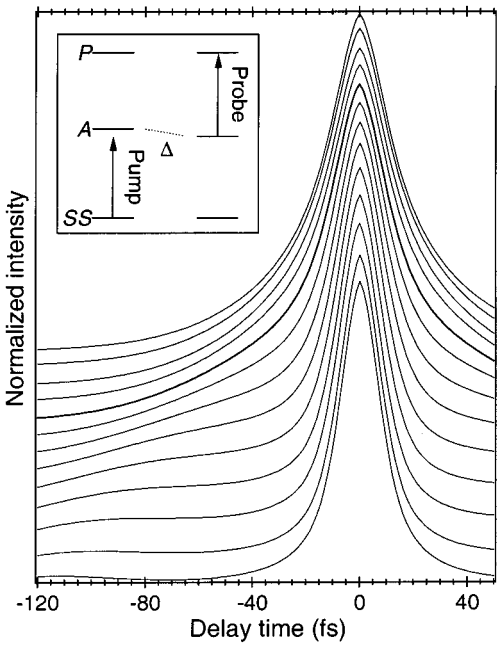

Figure 9. Simulated 0ω envelopes based on the OBE formalism assuming the three-level scheme in the inset, where the energy of the intermediate state decays quadratically with the delay. The simulation is performed in 25 meV intervals in decreasing energy order from top-to-bottom near the SS → A resonance. The thick line represents the simulation corresponding to the intensity maximum of *A*.

between the experiment and simulation is in the fast decay component, which arises from the exclusion of the bulk continuum contribution to 2PP from the OBE model. Thus, the incipient photodesorption of the Cs atoms provides the most intuitive and consistent interpretation for the observed dynamics.

E. Experimentally Derived Excited-State PES. Direct observation of the Cs atom motion provides unprecedented opportunity to derive experimental information on the PES for the photodesorption. Since τ_A is too short for substantial Cs atom motion, the object here is to estimate the slope of the potential at the point of the excitation, rather than to attempt a more complete reconstruction of the PES, because the 2PP data provide information only on short time dynamics. Although the wave packet can be monitored for up to ~200 fs, only the results for the first 50 fs are used, because, for $\Delta > 50$ fs, the difference spectra significantly increase in width and acquire structure, preventing a unique and unbiased determination of E_A.[26]

Deducing the excited-state PES from $E_A(\Delta)$ requires the consideration of how E_A relates to the potential energy, the appropriate choice for the effective mass for the Cs atom motion, and the role of dissipation. The energy required to bring a Cs atom to the metal surface is stored in the electronic and nuclear degrees of freedom of the adsorbate and the substrate. The leading term in this interaction is the upward shift and hybridization of the 6s orbital with $6p_z$ and other unoccupied orbitals of the Cs atom.[69] The experiment monitors the energy E_A of this transiently occupied orbital with respect to E_F during the process of desorption. Potential energy has other contributions, including the partially screened attraction of the Cs^+ core to the metal surface, Cs atom-induced rumpling of the surface, and the hybridization of other occupied orbitals of the Cs atom and the substrate that are not monitored in the experiment. Since the correspondence between the observed $E_A(\Delta)$ and PES is not known, the following procedure is adopted for deriving the PES.

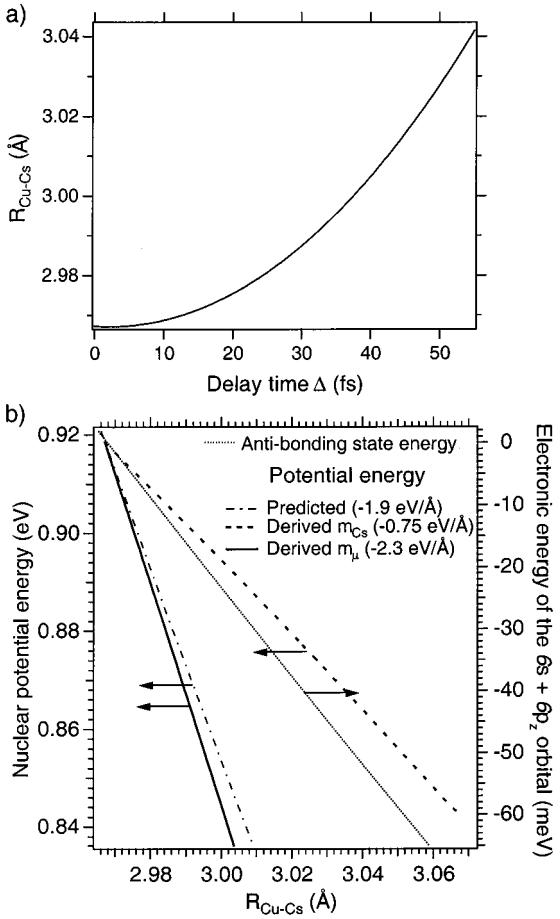

Figure 10. (a) Wave packet position as a function of delay as deduced from the difference spectra in Figure 8. (b) The predicted (short dot−dashed line; see Figure 1b) and derived potential energy surfaces (dashed line is for $m_\mu = m_{Cs}$, and solid line for $m\mu = m_{Cs}m_{Cu}/(m_{Cs} + m_{Cu})$) in the Franck−Condon region. The calculated change in the energy of the antibonding state as a function of R_{Cu-Cs} (dotted line)[58] is used to derive the curve in (a).

If the one-dimensional model in Figure 1b is appropriate for describing the Cs atom desorption, the $E_A(\Delta)$ data in Figure 8 can be transformed into the nuclear wave packet motion $R_{Cu-Cs}(\Delta)$, if $E_A(R_{Cu-Cs})$ is known. This transformation is accomplished in Figure 10a with the calculated $E_A(R_{Cu-Cs})$ from ref 58, which is reproduced in Figure 10b. Having obtained $R_{Cu-Cs}(\Delta)$, the slope of the dissociative potential is obtained as follows. The fitted curve in Figure 10a is differentiated to obtain the wave packet acceleration $\partial^2 R(\Delta)/\partial\Delta^2 = a$. Then the force $F = ma$ is integrated, i.e., $U = -\int F\, dR$, to derive the experimental PESs. This classical model explains the *nonexponential* I2PC decays in terms of changes in the surface electronic structure induced by stretching of the Cu−Cs bond by ~0.15 Å in 50 fs after excitation.[26]

In this one-dimensional model there is still one unknown parameter, namely, how the momentum is distributed among the recoiling particles. One limiting case is that of desorption from a rigid, infinitely massive wall, i.e., the potential energy is converted entirely into the kinetic energy of the Cs atom, and therefore, the mass of Cs atom is used to calculate the force. As shown in Figure 10b, this model predicts the slope of the excited-state PES at the point of vertical excitation of −0.75 eV/Å, as compared with predicted −1.9 eV/Å for the PES in Figure 1b. This large difference suggests that the actual potential is much softer than predicted in Figure 1b, or that Cs atoms recoil from a less rigid surface than assumed in this model. The

PES can be estimated in the opposite binary collision limit where Cs desorption is modeled as dissociation of a Cu−Cs diatomic molecule. In this limit, Cs receives the minimum kinetic energy because most of the energy is imparted to a single Cu atom that recoils with equal and opposite momentum. Although in the diatomic limit the acceleration $\partial^2R/\partial\Delta^2$ of Cs from its neighboring Cu atom is maximum, the electronic properties of Cs depend on its surface environment rather than just single Cu atom. Therefore, it is likely that the relevant motion for considering the electronic structure is that of the Cs atom with respect to the image plane, rather than to the recoiling Cu atom. In the binary collision limit the reduced mass $m_\mu = m_{Cs}/3.09$ for the relative motion of Cs with respect to Cu is appropriate for describing the wave packet motion. This results in a much steeper slope of the PES of −2.3 eV/Å, because the force exerted on the Cs atom must be proportionally larger to achieve equivalent momentum transfer as in the rigid, massive wall approximation. The slope of the potential is in much better agreement with the predicted PES in Figure 1b.

The agreement between the predicted PES and that derived from the binary collision model suggests that a substantial amount of potential energy available for desorption Cs atoms is deposited in the recoil of Cu atoms into the surface. However, the present case of scattering of a heavy atom from a light surface atom is in the opposite limit to where the binary collision model is likely to be valid.[123] For Cs on copper, not only is the mass ratio unfavorable but also the Cs atom is significantly larger than the Cu atom. This is especially true in the excited state where the electron distribution on the Cs atom covers several substrate atoms, as can be seen in figure 2 of ref 98, and therefore, desorption should simultaneously impart momentum to several substrate atoms. Although the difference between the binary collision and predicted potentials suggests that the effective mass of the recoiling particle is larger than that of a single Cu atom, extracting such information from the predicted slope is not deemed to be justified considering the unknown reliability of the predicted potential.

F. Photodesorption of Cs. Interpretation of the nonexponential decays in terms of the incipient Cs atom desorption provides a snapshot of the dynamics near the Franck−Condon region. Further information on the long time dynamics can be gleaned by monitoring the production of free Cs atoms or ions. The change in Φ with irradiation is a sensitive probe of Θ_{Cs}, which makes it possible to estimate the upper limit for the desorption yield as a function of irradiation dose. This procedure gives an upper limit for the photodesorption cross section of $\sigma_{Cs/Cu} < 2.4 \times 10^{-23}$ cm^2, which is to be compared with $\sigma_{K/C} = 2 \times 10^{-20}$ cm^2 for the desorption of K from graphite.[52] Unfortunately, $\sigma_{Cs/Cu}$ is too small to detect the Cs product by conventional electron-impact quadrupole mass spectroscopy. However, with a thermal ionization detector using on a Re ribbon, which has unity ionization efficiency and allows integration of desorbed Cs product on a cold Re surface, the sensitivity of Cs atom detection can be greatly enhanced.[82] This procedure confirms the Cs desorption, but the yield is too small for quantitative measurements.

G. Energy Dissipation. The present analysis contains several seemingly incongruous elements. On one hand, the antibonding state lifetime τ_A is unusually long and the slope of the postulated potential in Figure 1b is steep. On the other hand, $\sigma_{Cs/Cu}$ is vanishingly small. This conundrum can be reconciled by elaborating the MGR model.

The postulated PESs in Figure 1b, as in most treatments of surface photochemistry, approximate the desorption process as a one-dimensional "half-collision" of a Cs atom with a rigid wall of an infinite mass. However, even for light particles such as He atoms, the inelastic scattering process can involve multiple phonon excitation.[124] Thus, a more realistic description of Cs desorption should also consider the degrees of freedom involving the motion of the substrate Cu atoms as already introduced in the binary collision model. Since most of the potential energy is converted into kinetic energy of Cu atoms, only the remaining energy is available for desorption, unless Cs can gain further energy by multiple scattering the recoiling Cu atoms. This will not happen if the initial kinetic energy imparted to Cu atoms is lost to bulk phonons. The energy dissipation rate from the reaction coordinate is not known, but the decoherence rate of the antibonding state $\Gamma^A = 15^{-1}$ fs^{-1}, which appears to be a phonon-induced process, suggests that it could be significantly faster than the electronic relaxation of Cs atoms. The rapid loss of energy to recoiling Cu atoms is supported by scattering measurements of hyperthermal Xe atoms from a variety of metal and semiconductor surfaces, which show that most of the normal component of kinetic energy of a heavy scatterer is lost to the substrate phonons.[125,126] Thus, in the half-collision of 1 eV Cs atom with a copper surface, most of the available energy is used to deform the surface, and little is available for the recoil of the Cs atom. Therefore, the one-dimensional potential energy surface in Figure 1b fails to describe the multicenter scattering process whereby the Cu−Cs repulsion is converted into the outward Cs atom motion.

This refined picture of the Cs atom dynamics is consistent with the low photodesorption yield. The small value of $\sigma_{Cs/Cu}$ reflects both the long interaction of Cs atoms with the surface and inefficient coupling of the potential energy into the desorption coordinate. Cs atoms need to travel a substantial distance before accumulating sufficient kinetic energy for desorption from the ground state surface, according to the MGR scenario in Figure 1b. The probability of reaching the critical distance for desorption depends on both the Cs atom velocity as well as the lifetime. The moderate slope of the dissociative potential implies a slow and inefficient acceleration of Cs atoms from the copper surface. The ineffective transfer of momentum to Cs atoms implies a slow desorption velocity, which can compensate for the long lifetime resulting in a low photodesorption yield. An even more fundamental failing of the GMR scenario for heavy particle desorption from a light surface is that a significant fraction of the available energy is lost to substrate phonons, diminishing the available kinetic energy for desorption on the ground PES. Thus, both the slow acceleration and energy dissipation frustrate desorption of Cs atoms, despite the long residence time on the dissociative PES.

V. Conclusions

The photoinduced dynamics of alkali atoms on noble metal surfaces provide significant new insights into surface photochemical processes. Both the 2PP spectra and I2PC scans indicate that, at least for the chemisorption system of alkali atoms on noble metals, the photochemistry is initiated through the coherent charge transfer excitation, rather than the commonly invoked hot electron mechanism. The alkali atom antibonding state lifetimes greatly depend on electronic properties of the adsorbate and the substrate, such as the atomic polarizability and location of antibonding state within the projected band gaps of the metal substrate. The crystal face dependence of the adsorbate electronic relaxation rates suggests that presence of projected band gaps in metallic band structures can significantly affect the photochemical quantum yields. The considerable

difference between the phase and energy relaxation rates provides the first direct evidence that in some cases photoemission line widths may significantly overestimate the adsorbate state lifetimes. The photoinduced charge-transfer excitation creates neutral Cs atoms at the bonding distance from the surface. The resulting Coulomb repulsion initiates the nuclear wave packet motion leading to characteristic nonexponential decays and time dependent 2PP spectra. However, the loss of Cs atom kinetic energy to the substrate phonons frustrates the efficient desorption from the surface. Finally, insights gained from the dynamics of alkali atoms on noble metals offer guidance for exploring other chemisorption systems that might exhibit novel surface femtochemistry.

Acknowledgment. This work is dedicated to Prof. John T. Yates, Jr. in honor of his 65th birthday. The authors are indebted to S. Gao, J.-P. Gauyacq, T. F. Heinz, U. Höfer, D. Menzel, M. Wolf, and W. Wurth for insightful discussions into various aspects of surface photochemistry, surface charge transfer, and alkali atom chemisorption. M. Moria and S. Matsunami provided invaluable technical support in establishing the ITR-2PP experiments. Partial funding for this research has been provided by a NEDO Joint International Research Grant. M. J. Weida thanks the National Science Foundation and the Center for Global Partnership for support (NSF grant INT-9819100). H. Petek is grateful to the Alexander von Humboldt Foundation and H.-J. Freund for making possible his stay at the Fritz-Haber-Institute while completing this manuscript.

References and Notes

(1) Polanyi, J. C.; Zewail, A. H. *Acc. Chem. Res.* **1995**, *28*, 119.
(2) Zewail, A. H. *J. Phys. Chem. A* **2000**, *104*, 5660.
(3) Cong, P.; Roberts, G.; Herek, J. L.; Mohktari, A.; Zewail, A. H. *J. Phys. Chem.* **1996**, *100*, 7832.
(4) Fork, R. L.; Cruz, C. H. B.; Becker, P. C.; Shank, C. V. *Opt. Lett.* **1987**, *12*, 483.
(5) Baltuska, A.; Wei, Z.; Pshenichnikov, M. S.; Wiersma, D. A.; Szipöcs, R. *Appl. Phys. B* **1997**, *65*, 175.
(6) Scherer, N. F.; Carlson, R. J.; Matro, A.; Du, M.; Ruggiero, A. J.; Romero-Rochin, V.; Cina, J. A.; Fleming, G. R.; Rice, S. A. *J. Chem. Phys.* **1991**, *95*, 1487.
(7) Shapiro, M.; Brumer, P. *J. Chem. Soc., Faraday Trans.* **1997**, *93*, 1263.
(8) Assion, A.; Baumert, T.; Bergt, M.; Brixner, T.; Kiefer, B.; Seyfried, V.; Strehle, M.; Gerber, G. *Science* **1998**, *282*, 919.
(9) Cavanagh, R. R.; King, D. S.; Stephenson, J. C.; Heinz, T. F. *J. Phys. Chem.* **1993**, *97*, 786.
(10) Zhu, X.-Y. *Annu. Rev. Chem. Phys.* **1994**, *45*, 113.
(11) Zimmermann, F. M.; Ho, W. *Surf. Sci. Rep.* **1995**, *22*, 127.
(12) *Laser Spectroscopy and Photochemistry on Metal Surfaces*; Dai, H.-L., Ho, W., Eds.; World Scientific: Singapore, 1995; Vol. 5.
(13) Ho, W. *Acc. Chem. Res.* **1998**, *31*, 567.
(14) Gadzuk, J. W. *Surf. Sci.* **1995**, *342*, 345.
(15) Saalfrank, P.; Darling, G.; Holloway, S. *J. Chem. Phys.* **1995**, *103*, 6720.
(16) Klüner, T.; Freund, H.-J.; Staemmler, V.; Kosloff, R. *Phys. Rev. Lett.* **1998**, *80*, 5208.
(17) Hasselbrink, E. State-Resolved Probes of Molecular Desorption Dynamics Induced by Short-Lived Electronic Excitations. In *Laser Spectroscopy and Photochemistry on Metal Surfaces*; Dai, H. L., Ho, W., Eds.; World Scientific: Singapore, 1995; Vol. II.; p 685.
(18) Bartels, L.; Meyer, G.; Rieder, K.-H.; Velic, D.; Knoesel, E.; Hotzel, A.; Wolf, M.; Ertl, G. *Phys. Rev. Lett.* **1998**, *80*, 2004.
(19) Bauer, M.; Pawlik, S.; Aeschlimann, M. *Phys. Rev. B* **1997**, *55*, 10040.
(20) Bauer, M.; Pawlik, S.; Burgermeister, R.; Aeschlimann, M. *Surf. Sci.* **1998**, *402*−*404*, 62.
(21) Bauer, M.; Pawlik, S.; Aeschlimann, M. *Phys. Rev. B* **1999**, *60*, 5016.
(22) Ogawa, S.; Nagano, H.; Petek, H. *Phys. Rev. Lett.* **1999**, *82*, 1931.
(23) Ogawa, S.; Nagano, H.; Petek, H. *Appl. Phys. B* **1999**, *68*, 611.
(24) Ogawa, S.; Nagano, H.; Petek, H. *Surf. Sci.* **1999**, *427/428*, 34.
(25) Petek, H.; Weida, M. J.; Nagano, H.; Ogawa, S. *Surf. Sci.* **2000**, *451*, 22.
(26) Petek, H.; Nagano, H.; Weida, M. J.; Ogawa, S. *Science* **2000**, *288*, 1402.
(27) Petek, H.; Weida, M. J.; Nagano, H.; Ogawa, S. *J. Phys. Chem. A* **2000**, *104*, 10234.
(28) Menzel, D.; Gomer, R. *J. Chem. Phys.* **1964**, *41*, 3311.
(29) Redhead, P. A. *Can. J. Phys.* **1964**, *42*, 886.
(30) Antoniewicz, P. R. *Phys. Rev. B* **1980**, *21*, 3811.
(31) Gadzuk, J. W. *Chem. Phys.* **2000**, *251*, 87.
(32) Weik, F.; Meijere, A. d.; Hasselbrink, E. *J. Chem. Phys.* **1993**, *99*, 682.
(33) Richter, L. J.; Buntin, S. A.; King, D. S.; Cavanagh, R. R. *Chem. Phys. Lett.* **1991**, *186*, 423.
(34) Watanabe, K.; Sawabe, K.; Matsumoto, Y. *Phys. Rev. Lett.* **1996**, *76*, 1751.
(35) Gusev, V. E.; Wright, O. B. *Phys. Rev. B* **1998**, *57*, 2878.
(36) Bonn, M.; Denzler, D. N.; Funk, S.; Wolf, M.; Wellershoff, S.-S.; Hohlfeld, J. *Phys. Rev. B* **2000**, *61*, 1101.
(37) Bourdon, E. B. D.; Cowin, J. P.; Harrison, I.; Polanyi, J. C.; Segner, J.; Stanners, C. D.; Young, P. A. *J. Phys. Chem.* **1984**, *88*, 6100.
(38) So, S. K.; Ho, W. *J. Chem. Phys.* **1991**, *95*, 656.
(39) Mieher, W. D.; Ho, W. *J. Chem. Phys.* **1993**, *99*, 9279.
(40) Hellsing, B. *Surf. Sci.* **1993**, *282*, 216.
(41) Zacharias, H.; Eichhorn, G.; Schliesing, R.; Al-Shamery, K. *Appl. Phys. B* **1999**, *68*, 605.
(42) Wolf, M.; Hotzel, A.; Knoesel, E.; Velic, D. *Phys. Rev. B* **1999**, *59*, 5926.
(43) Saalfrank, P.; Kosloff, R. *J. Chem. Phys.* **1996**, *105*, 2441.
(44) Knoesel, E.; Hertel, T.; Wolf, M.; Ertl, G. *Chem. Phys. Lett.* **1995**, *249*, 409.
(45) Munakata, T.; Sakashita, T.; Tsukakoshi, M.; Nakamura, J. *Surf. Sci.* **1996**, *357/358*, 629.
(46) Avouris, P.; Schmeisser, D.; Demuth, J. E. *J. Chem. Phys.* **1983**, *79*, 488.
(47) Smith, N. V.; Thiry, P.; Petroff, Y. *Phys. Rev. B* **1993**, *47*, 15476.
(48) McDougall, B. A.; Balasubramanian, T.; Jensen, E. *Phys. Rev. B* **1995**, *51*, 13891.
(49) Knoesel, E.; Hotzel, A.; Wolf, M. *J. Electron Spectrosc. Relat. Phenom.* **1998**, *88*−*91*, 577.
(50) Petek, H.; Nagano, H.; Ogawa, S. *Phys. Rev. Lett.* **1999**, *83*, 832.
(51) Cho, M.; Scherer, N. F.; Fleming, G. R.; Mukamel, S. *J. Chem. Phys.* **1992**, *96*, 5618.
(52) Hellsing, B.; Chakarov, D. V.; Österlund, L.; Zhadanov, V. P.; Kasemo, B. *J. Chem. Phys.* **1996**, *106*, 982.
(53) Petek, H.; Ogawa, S. *Prog. Surf. Sci.* **1997**, *56*, 239.
(54) Schneider, R.; Dürr, H.; Fauster, T.; Dose, V. *Phys. Rev. B* **1990**, *42*, 1638.
(55) Dietz, E.; Himpsel, F. J. *Solid State Commun.* **1979**, *30*, 235.
(56) Eckardt, H.; Fritsche, L.; Noffke, J. *J. Phys. F* **1984**, *14*, 97.
(57) Matzdorf, R. *Surf. Sci. Rep.* **1997**, *30*, 153.
(58) Borisov, A. G.; Kazansky, A. K.; Gauyacq, J. P. *Surf. Sci.* **1999**, *430*, 165.
(59) Gurney, R. W. *Phys. Rev.* **1935**, *47*, 479.
(60) Muscat, J. P.; Newns, D. M. *Surf. Sci.* **1978**, *74*, 355.
(61) Muscat, J. P.; Newns, D. M. *Surf. Sci.* **1979**, *84*, 262.
(62) Muscat, J. P.; Newns, D. M. *Prog. Surf. Sci.* **1978**, *9*, 1.
(63) Ishida, H. *Phys. Rev. B* **1988**, *38*, 8006.
(64) Ishida, H. *Phys. Rev. B* **1989**, *39*, 5492.
(65) Ishida, H.; Liebsch, A. *Phys. Rev. B* **1992**, *45*, 6171.
(66) Wertheim, G. K.; Riffe, D. M.; Citrin, P. H. *Phys. Rev. B* **1994**, *49*, 4834.
(67) Diehl, R. D.; McGrath, R. *J. Phys. C* **1997**, *9*, 951.
(68) Bormet, J.; Neugebauer, J.; Scheffler, M. *Phys. Rev. B* **1994**, *49*, 17242.
(69) Nordlander, P.; Tully, J. C. *Phys. Rev. B* **1990**, *42*, 5564.
(70) Lang, N. D.; Williams, A. R. *Phys. Rev. B* **1978**, *18*, 616.
(71) Langmuir, I. *Phys. Rev.* **1933**, *43*, 224.
(72) Woratschek, B.; Sesselmann, W.; Küppers, J.; Ertl, G.; Haberland, H. *Phys. Rev. Lett.* **1985**, *55*, 1231.
(73) Sandell, A.; Hjortstam, O.; Nilsson, A.; Brühwiler, P. A.; Eriksson, O.; Bennich, P.; Rudolf, P.; Wills, J. M.; Johansson, B.; Mårtensson, N. *Phys. Rev. Lett.* **1997**, *78*, 4994.
(74) Sandell, A.; Brühwiler, P. A.; Nilsson, A.; Bennich, P.; Rudolf, P.; Mårtensson, N. *Surf. Sci.* **1999**, *429*, 309.
(75) Lou, L.; Österlund, L.; Hellsing, B. *J. Chem. Phys.* **2000**, *112*, 4788.
(76) Frank, K.-H.; Sagner, H.-J.; Heskett, D. *Phys. Rev. B* **1989**, *40*, 2767.
(77) Arena, D. A.; Curti, F. G.; Bartynski, R. A. *Phys. Rev. B* **1997**, *56*, 15404.
(78) Haskett, D.; Frank, K.-H.; Horn, K.; Koch, E. E.; Freund, H.-J.; Baddorf, A.; Tsuei, K.-D.; Plummer, E. W. *Phys. Rev. B* **1988**, *37*, 10387.
(79) Lindgren, S. Å.; Walldén, L. *Phys. Rev. B* **1992**, *45*, 6345.
(80) Fischer, N.; Schuppler, S.; Fauster, T.; Steinmann, W. *Surf. Sci.* **1994**, *314*, 89.

(81) Ishida, H.; Liebsch, A. *Phys. Rev. B* **1990**, *42*, 5505.
(82) Yakshinskiy, B. V.; Madey, T. E. *Nature* **1999**, *400*, 642.
(83) Wilde, M.; Beauport, I.; Stuhl, F.; Al-Shamery, K.; Freund, H.-J. *Phys. Rev. B* **1999**, *59*, 13401.
(84) Stolz, H.; Hüfer, M.; Wassmuth, H.-W. *Surf. Sci.* **1993**, *286/287*, 564.
(85) Shih, A.; Parsegian, V. A. *Phys. Rev. A* **1975**, *12*, 835.
(86) Weida, M. J.; Ogawa, S.; Nagano, H.; Petek, H. *Appl. Phys. A* **2000**, *71*, 553.
(87) Weida, M. J.; Ogawa, S.; Nagano, H.; Petek, H. *J. Opt. Soc. Am. B* **2000**, *17*, 1443.
(88) Ogawa, S.; Nagano, H.; Petek, H.; Heberle, A. *Phys. Rev. Lett.* **1997**, *78*, 1339.
(89) Ondrejcek, M.; Chab, V.; Stenzel, W.; Snabl, M.; Conrad, H.; Bradshaw, A. M. *Surf. Sci.* **1995**, *331*−*333*, 764.
(90) Petek, H.; Heberle, A. P.; Nessler, W.; Nagano, H.; Kubota, S.; Matsunami, S.; Moriya, N.; Ogawa, S. *Phys. Rev. Lett.* **1997**, *79*, 4649.
(91) Gumhalter, B.; Petek, H. *Surf. Sci.* **2000**, *445*, 195.
(92) Beckmann, A. *Surf. Sci.* **1994**, *326*, 335.
(93) Petek, H.; Nagano, H.; Weida, M.; Ogawa, S. *Chem. Phys.* **2000**, *251*, 71.
(94) Ogawa, S.; Nagano, H.; Petek, H. *Phys. Rev. B* **1997**, *55*, 10869.
(95) Goldmann, A.; Matzdorf, R.; Theilmann, F. *Surf. Sci.* **1998**, *414*, L932.
(96) Knapp, J. A.; Himpsel, F. J.; Eastman, D. E. *Phys. Rev. B* **1979**, *19*, 4952.
(97) In ref 21, Bauer et al., however, do not see the resonance enhancement when the SS → A transition and photon energies coincide, and hence conclude that the initial states are the bulk bands of the substrate. The reason the resonance enhancement is not observed is not clear, but probably arises from different experimental conditions.
(98) Borisov, A. G.; Gauyacq, J. P.; Kazansky, A. K.; Chulkov, E. V.; Silkin, V. M.; Echenique, P. M. *Phys. Rev. Lett.* **2001**, *86*, 488.
(99) Gauyacq, J. P.; Borisov, A. G.; Raseev, G.; Kazansky, A. K. *Faraday Discuss. Chem. Soc.* **2000**, *117*.
(100) Keller, C.; Stichler, M.; Comelli, G.; Esch, F.; Lizzit, S.; Menzel, D.; Wurth, W. *Phys. Rev. B* **1998**, *57*, 11951.
(101) In ref 21 Bauer et al. report broadening of the two-pulse correlation scans, which they attribute to 6 ± 4 fs lifetime of the antibonding state for Cs/Cu(100). No such broadening of the I2PC scans could be detected in higher time resolution experiments performed here.
(102) Osma, J.; Sarría, I.; Chulkov, E. V.; Pitarke, J. M.; Echenique, P. M. *Phys. Rev. B* **1999**, *59*, 10591.
(103) Borisov, A. G.; Kazansky, A. K.; Gauyacq, J. P. *Phys. Rev. Lett.* **1998**, *80*, 1996.
(104) Fauster, T.; Steinmann, W. Two-photon photoemission spectroscopy of image states. In *Electromagnetic Waves: Recent Developments in Research*; Halevi, P., Ed.; Elsevier: Amsterdam, 1994; Vol. 2, p 1.
(105) Schoenlein, R. W.; Fujimoto, J. G.; Eesley, G. L.; Capehart, T. W. *Phys. Rev. B* **1991**, *43*, 4688.
(106) Höfer, U.; Shumay, I. L.; Reuss, C.; Thomann, U.; Wallauer, W.; Fauster, T. *Science* **1997**, *277*, 1480.
(107) Ramakrishna, R.; Willig, F.; May, V. *Phys. Rev. B* **2000**, *62*, R16330.
(108) Beard, M. C.; Turner, G. M.; Schmuttenmaer, C. A. *J. Am. Chem. Soc.* **2000**, *122*, 11541.
(109) Persson, B. N. J.; Dubois, L. H. *Phys. Rev. B* **1989**, *39*, 8220.
(110) Senet, P.; Toennies, J. P.; Witte, G. *Chem. Phys. Lett.* **1999**, *299*, 389.
(111) Meyerheim, H. L.; Weaver, J.; Jahns, V.; Moritz, W.; Eng, P. J.; Robinson, I. K. *Surf. Sci.* **1994**, *304*, 267.
(112) Kim, Y. K.; Rundgren, J.; Over, H., to be published.
(113) Caragiu, M.; Leatherman, G. S.; Diehl, R. D.; Kaukasoina, P.; Lindroos, M. *Surf. Sci.* **1999**, *441*, 84.
(114) Okada, M.; Tochihara, H.; Murata, Y. *Surf. Sci.* **1991**, *245*, 380.
(115) Fan, W. C.; Ignatiev, A. *J. Vac. Sci. Technol. A* **1988**, *6*, 735.
(116) Thiel, P. A.; Madey, T. E. *Surf. Sci. Rep.* **1987**, *7*, 211.
(117) Hess, C.; Wolf, M.; Bonn, M. *Phys. Rev. Lett.* **2000**, *85*, 4341.
(118) Ge, N.-H.; Wong, C. M.; Lingle, R. L.; McNeil, J. D.; Gaffney, K. J.; Harris, C. B. *Science* **1998**, *279*, 202.
(119) Bonn, M.; Hess, C.; Miners, J. H.; Heinz, T. F.; Bakker, H. J.; Cho, M. *Phys. Rev. Lett.* **2001**, *86*, 1566.
(120) Levinson, H. J.; Plummer, E. W. *Phys. Rev. B* **1981**, *24*, 628.
(121) Wolf, M. *Surf. Sci.* **1997**, *377*−*379*, 343.
(122) Salour, M. M.; Cohen-Tannoudji, C. *Phys. Rev. Lett.* **1977**, *38*, 757.
(123) Sosolik, C. E.; Cooper, B. H. *Nucl. Instrum. Methods Phys. B*, in press.
(124) Gumhalter, B.; Langreth, D. C. *Phys. Rev. B* **1999**, *60*, 2789.
(125) Amirav, A.; Cardillo, M. J.; Trevor, P. L.; Lim, C.; Tully, J. C. *J. Chem. Phys.* **1987**, *87*, 1796.
(126) Winters, H. F.; Coufal, H.; Rettner, C. T.; Bethune, D. S. *Phys. Rev. B* **1990**, *41*, 6240.